This article has been accepted for publication in a future issue of this journal, but has not been fully edited. Content may change prior to final publication. Citation information: DOI 10.1109/TMECH.2019.2931407, IEEE/ASME Transactions on Mechatronics

Finite-Time Learning Control Using Frequency Response Data with Application to a Nanopositioning Stage

Robin de Rozario[1], Andrew Fleming[2] and Tom Oomen[1]

***Abstract*—Learning control enables significant performance improvement for systems that perform repeating tasks. Achieving high tracking performance by utilizing past error data typically requires noncausal learning that is based on a parametric model of the process. Such model-based approaches impose significant requirements on modeling and filter design. This paper aims to reduce these requirements by developing a learning control framework that enables performance improvement through noncausal learning without relying on a parametric model. This is achieved by explicitly using the discrete Fourier transform to enable learning by using a nonparametric frequency response function model of the process. The effectiveness of the developed method is illustrated by application to a nanopositioning stage.**

I. Introduction

Learning from error data that is obtained from past operations is an effective approach to improve the performance of mechatronic systems that perform repetitive tasks, including nanopositioning devices [1], industrial printers [2], and additive manufacturing systems [3]. More specifically, Repetitive Control (RC) can be applied to reduce tracking error in applications that operate in a continuous fashion [4], [5], whereas Iterative Learning Control (ILC) enables performance improvement for systems that operate in a batch-to-batch manner [6]–[9].

Parametric models are often employed in the design of RC and ILC controllers to achieve high convergence speeds. Fast convergence is obtained when the learning filter closely approximates the inverse system dynamics [10], [11]. Consequently, typical learning filter design approaches are based on inverting a parametric plant model [12]. However, special measures are required to ensure that the inverse of a Non-Minimum Phase (NMP) model is stable. More specifically, NMP zeros imply that a causal and stable inverse of the system does not exist and that a stable inverse is instead anti-causal [13]. For an anti-causal inverse, the input corresponding to the desired output can be determined through a process known as stable inversion [14]. Though, determining the exact inverse response requires infinite previewing of the desired output. Consequently, methods that approximate inverse Linear Time-Invariant (LTI) dynamics with a finite amount preview have received considerable attention [12], [15]–[17]. Since these methods are inherently model-based, significant requirements are imposed on learning filter design in terms of parametric identification and approximate inversion.

Iterative Inversion-based Control (IIC) is a related method that avoids the need for parametric models and seems to overcome the limitations related to bounded inversion. Aside from the robustness filter that was initially omitted in IIC [18], the IIC method [19] appears theoretically similar to infinite-time frequency-domain ILC [20], yet the two methods differ substantially in their implementation. In ILC, updating of the input signal is typically performed by using filtering operations, whereas, in IIC, the updating is performed by using the Discrete Fourier Transform (DFT). The latter enables the use of nonparametric Frequency Response Function (FRF) models, thereby removing the need for parametric models. This approach is shown to be effective [21]–[23] and seems to inherently facilitate noncausal learning with bounded inputs [24], [25], yet a full analysis of the potential limitations imposed by NMP zero dynamics has not yet been established.

In practice, the IIC method is typically implemented in discrete finite time and is reported to accommodate both batch-to-batch and continuous processes. Pre-existing analyses of IIC assume that the system is in steady state. This can be approximately achieved in batch-to-batch processes by including trailing zeros [19], or by measuring only the final periods of a periodic task [21]. In this way, updating the input can be performed offline, as is characteristic of ILC. Similarly, measuring the steady state of a continuous process can be approximately achieved by waiting for some time after the input was last updated [26]. In this way, the input can be updated while the process operates continuously, as is characteristic of RC. In practice, however, the process is never truly in steady state, and pre-existing analyses do not provide clear guidelines to address the waiting period that is required to avoid the instability incurred by residual transients.

Although significant progress has been made to reduce the modeling and design requirements in learning control, at present, a systematic approach for fast and robust learning for NMP systems is not yet established. This paper aims to fill this gap by developing a finite-time FRF-based learning control framework, supported by key analyses that are lacking in the present literature. This is achieved in combination with the following contributions.

(C1) A method is developed to stably invert an NMP LTI system by using its FRF (Section III).

(C2) A robust finite-time IIC approach is developed (Section II), and guidelines are derived to achieve high performance and robustness against uncertainties (Section IV).

[1]Faculty of Mechanical Engineering, Control Systems Technology, Eindhoven University of Technology, 5600 MB Eindhoven, The Netherlands, r.d.rozario@tue.nl, t.a.e.oomen@tue.nl

[2]University of Newcastle, Electrical and Computer Engineering, Australia andrew.fleming@newcastle.edu.au. This work is supported by Océ Technologies and by the Netherlands Organization for Scientific Research (NWO) through research program VIDI under project 15698.

This article has been accepted for publication in a future issue of this journal, but has not been fully edited. Content may change prior to final publication. Citation information: DOI 10.1109/TMECH.2019.2931407, IEEE/ASME Transactions on Mechatronics

(C3) A finite-time analysis of the developed approach is established to determine the waiting period that is required to achieve convergence, and it is shown how the developed approach relates to ILC and RC (Section V).

(C4) The effectiveness of the developed method is confirmed by applying it to control a nanopositioner in the continuous implementation setting (Section VI).

These contributions extend pre-existing IIC as follows. First, contribution C1 motivates the use of FRF models in learning by showing that stable inversion of NMP systems can readily be achieved in the frequency domain [14], [27]. Second, contribution C2 incorporates robustness by explicitly considering convergence in the presence of uncertainties in the FRF data. Third, contribution C3 provides guidelines for the effective implementation of IIC in finite time by considering the effect of the transient response on the convergence.

This article extends the initial research reported in [18] by significantly extending contribution C2, adding contributions C1 and C3, and by providing rigorous proofs of the results.

A. Notation

The set of real numbers, complex numbers, and integers are denoted by $\mathbb{R}$, $\mathbb{C}$, and $\mathbb{Z}$. The nonnegative real line, the unit circle, and the complex right half plane are denoted by $\mathbb{R}_{\geq 0} = [0, \infty)$, $\mathbb{C}^\circ \triangleq \{\xi \in \mathbb{C} \,|\, |\xi| = 1\}$ and $\mathbb{C}_{>0} \triangleq \{\xi \in \mathbb{C} \,|\, \Re\{\xi\} > 0\}$. For a Discrete Time (DT) signal $f : \mathbb{Z} \mapsto \mathbb{R}$, the norms of f are defined as $\|f\|_p^p = \sum_{t=-\infty}^{\infty} |f(t)|^p$ and $\|f\|_\infty = \max_{t\in\mathbb{Z}} |f(t)|$ and f is called N-periodic if $f(t+N) = f(t)\ \forall t \in \mathbb{Z}$, with $N \in \mathbb{N}$. The spaces with bounded $\|.\|_p$ and $\|.\|_\infty$ norms are denoted by ℓ_p and ℓ_∞. The Discrete Time Fourier Transform (DTFT) and its inverse are denoted by $\mathcal{F}_\infty$ and $\mathcal{F}_\infty^{-1}$ [28, §2.12]. The Discrete Fourier Transform (DFT) and its inverse are denoted by $\mathcal{F}_N$ and $\mathcal{F}_N^{-1}$ and are defined as $S(k) = \mathcal{F}_N\{s(t)\} \triangleq \frac{1}{\sqrt{N}} \sum_{t=0}^{N-1} s(t) e^{-j\omega_k t}$, $s(t) = \mathcal{F}_N^{-1}\{S(k)\} \triangleq \frac{1}{\sqrt{N}} \sum_{k=0}^{N-1} S(k) e^{j\omega_k t}$, $\omega_k = \frac{2\pi k}{N}$, $k = 0, 1, ..., N-1$ [28, §2.21]. Moreover, $[A]_{ij}$ denotes the ij-th element of the matrix $A \in \mathbb{C}^{n\times m}$, $A^H \triangleq \bar{A}^T$, with $\bar{A}$ the complex conjugate of A, and $\bar{\rho}(A)$ and $\bar{\sigma}(A)$ represent the largest eigenvalue and largest singular value of A. Additionally, $\mathrm{diag}\{s(k)\}$ is a diagonal matrix whose k-th diagonal equals $s(k)$. In this article, a single-input single-output LTI DT system G is considered, which is represented by a minimal realization

$$G : \left[\begin{array}{c|c} A & B \\ \hline C & D \end{array}\right] = \begin{cases} x(t+1) = Ax(t) + Bu(t), & \text{(1a)} \\ y(t) = Cx(t) + Du(t), & \text{(1b)} \end{cases}$$

where $x(t) \in \mathbb{R}^{n_x}$, $u(t), y(t) \in \mathbb{R}$ are the state vector, input and output. The corresponding transfer function is given by $G(z) = C(zI - A)^{-1}B + D$ and G is stable iff $\bar{\rho}(A) < 1$. Moreover, s_i denotes s at the i-th iteration.

II. Finite-time IIC

In this section, the tracking control problem is introduced, which is motivated by high-speed Scanning Probe Microscopy (SPM) systems. The Finite-Time IIC (FT-IIC) method is formulated as a solution to this problem and is subjected to rigorous analysis in the next sections.

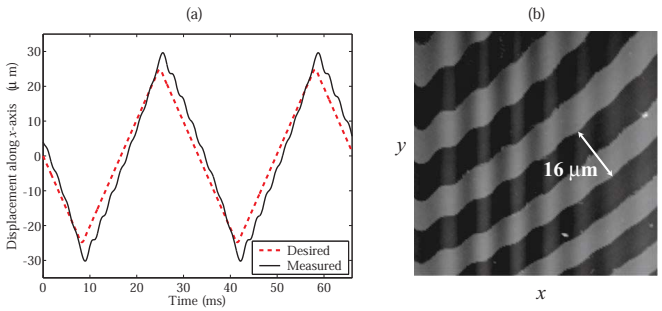

Fig. 1. The effect of positioning errors on the image quality in AFM: (a) actual and desired probe displacement over time, and (b) a distorted image (the actual features are parallel lines) [30, §2.6].

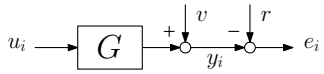

Fig. 2. The control configuration with exogenous output disturbances.

A. Application motivation

In SPM, such as scanning tunneling microscopy and atomic force microscopy, control is crucial to achieving accurate and fast positioning of the probe with respect to the sample [25], and largely determines the quality of the resulting images [29], as is illustrated in Figure 1. In typical SPM applications, the probe or sample is required to perform a periodic scanning motion. Commonly, the mechanical resonance frequencies of the positioning stage are in the same range as the desired scan rate, such that achieving an acceptable bandwidth using traditional feedback approaches is challenging [25], [30]. Furthermore, the system dynamics may vary due to variations in a sample's size and weight.

B. Problem formulation

Given the control challenges in SPM, it is desired that the developed method satisfies the following requirements.

(R1) Periodic references are accurately tracked and unknown periodic disturbances are rejected.

(R2) Convergence is achieved despite plant uncertainties.

(R3) A parametric model of the system is not required.

(R4) No additional measures are required to control systems with NMP zeros.

Motivated by the application to SPM, the following assumptions are made.

(A1) The process G is a stable LTI system with output disturbance $v(t)$, such that $y_i(t) = G(z)u_i(t) + v(t)$, as is shown in Figure 2.

(A2) The reference r is N-periodic and bounded.

(A3) The number of samples per period N is known.

Despite the hysteresis that is induced by piezo-based actuation in SPM applications [21], Assumption A1 is commonly made [25] and is especially accurate when a stabilizing feedback controller is employed that partly linearizes the system, as is briefly discussed in Section VI.

The problem of iteratively improving the tracking performance of periodic references is formulated as follows.

This article has been accepted for publication in a future issue of this journal, but has not been fully edited. Content may change prior to final publication. Citation information: DOI 10.1109/TMECH.2019.2931407, IEEE/ASME Transactions on Mechatronics

Problem 1. *Given an N-periodic reference $r(t)$, define*

$$e_i(t) \triangleq r(t) - y_i(t), \tag{2}$$

where $y_i(t)$ is as given in assumption A1, and $G(z)$ is given by (1)*. Determine a sequence of N-periodic inputs $\{u_i(t)\}_{i=0}^{\infty}$ such that $\lim_{i\to\infty} e_i(t)$ is small in an appropriate sense.*

In the next section, a frequency domain approach is proposed as a solution to this periodic tracking problem.

C. Finite Time Iterative Inversion-based Control

The following update law represents the proposed FT-IIC method, which aims to provide a solution to Problem 1 using an FRF model of the process.

Proposition 1. *Given an initial input $U_0(k)$, update U_i as,*

$$U_{i+1}(k) = Q(k)\left(U_i(k) + \alpha(k)\hat{G}^{-1}(k)E_i(k)\right), \quad \forall k, \tag{3}$$

where $\hat{G}(k)$ is an FRF model of $G(e^{j\omega_k})$ that satisfies $\hat{G}(k) \neq 0\ \forall k$, and $Q(k) \in \mathbb{R}_{\geq 0}$ and $\alpha(k) \in \mathbb{R}_{\geq 0}$ are referred to as the robustness and learning coefficient, respectively.

The key attribute of FT-IIC is the explicit use of the DFT to update the input. This enables the use of the nonparametric FRF model $\hat{G}(k)$ and ensures the satisfaction of requirement R3. This is essentially different from typical ILC approaches in which the update is performed by filtering the time domain signals [6]. The FRF model $\hat{G}(k)$ is typically considered to be a reliable approximation of the plant and its accuracy can be quantified using various techniques [31]. The coefficients $Q(k)$ and $\alpha(k)$ are used to enable robust convergence and to regulate the learning speed. These coefficients can be tuned separately for each frequency by assuming that the output is approximately in steady state, since, if $Y(k) \approx G(e^{j\omega_k})U(k)$, then the evolution of $U_i(k)$ for frequency k is independent of all other frequencies. This approach is enabled by the following implementation framework, where the distinction between batch-to-batch and continuous updating is made explicit in Section V-A and Figure 3 and 4.

Algorithm 1 FT-IIC

Select a suitable initial periodic input $u_0(t)$.

1) **Batch-to-batch**: reset the system to a certain initial x_0. **Continuous**: do not reset the system.
2) Apply the N-periodic input $u_i(t)$ to the system and wait w periods until the output $y_i(t)$ is approximately in steady state. Then, record the tracking error $e_i(t)$ (2).
3) a) Obtain $U_i(k)$ and $E_i(k)$ by applying the DFT.
   b) Update $U_i(k)$ using (3) for each frequency k.
   c) Obtain $u_{i+1}(t)$ by applying the IDFT.
4) Set $i \leftarrow i+1$. Repeat from 1) until $e_i(t)$ has converged.

Remark 1. *The results in this article apply to N-periodic and time-limited signals [28], since the DFT is an inherent part of FT-IIC. Time-limited tasks are naturally implemented in a batch-to-batch fashion resulting in $w = 0$. Furthermore, for $N \to \infty$ the classical IIC and infinite-time ILC methods are reobtained.*

D. Outline

The remainder of this article is structured as follows. In light of requirement R4, it is shown in Section III that (3) results in bounded inputs, even when $G(z)$ is NMP. In Section IV, the convergence behavior and asymptotic properties of (3) are derived under the assumption that the system is in steady state, which results in tuning guidelines for $Q(k)$ and $\alpha(k)$ to satisfy requirements R1 and R2. In Section V, finite-time effects are explicitly analyzed using a lifted signal framework, which results in conditions on the number of waiting periods w to ensure convergence. In Section VI, the developed FT-IIC method is applied to a nanopositioning stage.

III. Fourier Transform-based Stable Inversion

In this section, it is shown that in contrast to inverse-model-based learning, the presented inverse-FRF-based approach results in bounded signals, irrespective of the potential presence of NMP dynamics. This is shown by explicitly solving the stable inversion problem in the frequency domain, which constitutes contribution C1. More specifically, this section aims to derive conditions under which

$$u(t) = \mathcal{F}_N^{-1}\{G^{-1}(k)\mathcal{F}_N\{r(t)\}\},$$

is guaranteed to be bounded while satisfying $y(t) = r(t)$.

A. Stable inversion in the time domain

The stable inversion problem is first considered in the time domain. Considering (2) for $v(t) = 0$ shows that the perfect tracking input is obtained by inverting the relation $Gu = r$. Ensuring that $u(t)$ is bounded is known as the problem of stable inversion, which is formulated as follows [14].

Problem 2 (Stable inversion)**.** *Let $G : u \mapsto y$ be a DT-LTI system. Then, for a certain $r \in \ell_\infty$, determine $u \in \ell_\infty$ such that* (1) *holds in addition to $y(t) = r(t)\ \forall t \in \mathbb{Z}$.*

A time domain solution [14] follows by inverting the state-space realization of G, i.e., (1), which is given by

$$G^{-1} : \left[\begin{array}{c|c} \tilde{A} & \tilde{B} \\ \hline \tilde{C} & \tilde{D} \end{array}\right] = \left[\begin{array}{c|c} A - BD^{-1}C & BD^{-1} \\ \hline -D^{-1}C & D^{-1} \end{array}\right].$$

Note that this can be extended to the case with $D = 0$ by using input- or output previewing [32]. When G is NMP, at least one of the zeros of $G(z)$ lies outside of the unit circle. This renders G^{-1} unstable in a causal sense since the zeros of G are equal to the poles of G^{-1}. If none of the eigenvalues of $\tilde{A}$ lie on the unit circle, a similarity transformation $\eta = T\tilde{x}$ can be performed that decouples the dynamics in a stable and anti-stable part [14]. This dichotomous split results in

$$G^{-1} : \begin{cases} \begin{bmatrix} \eta_s(t+1) \\ \eta_u(t+1) \end{bmatrix} = \begin{bmatrix} \tilde{A}_s & 0 \\ 0 & \tilde{A}_u \end{bmatrix} \begin{bmatrix} \eta_s(t) \\ \eta_u(t) \end{bmatrix} + \begin{bmatrix} \tilde{B}_s \\ \tilde{B}_u \end{bmatrix} y(t), \\ u(t) = \begin{bmatrix} \tilde{C}_s & \tilde{C}_u \end{bmatrix} \eta(t) + \tilde{D}y(t). \end{cases}$$

A bounded yet noncausal u is obtained by iterating η_s forward in time, and η_u backward in time for $y = r$, i.e.,

$$\eta_s(t) = \sum_{i=-\infty}^{t-1} \tilde{A}_s^{t-i-1} B_s y(i), \quad \eta_u(t) = -\sum_{i=t}^{\infty} \tilde{A}_u^{t-i-1} B_u y(i).$$

This article has been accepted for publication in a future issue of this journal, but has not been fully edited. Content may change prior to final publication. Citation information: DOI 10.1109/TMECH.2019.2931407, IEEE/ASME Transactions on Mechatronics

This approach solves Problem 2 if G has neither zeros nor poles on $\mathbb{C}^\circ$ [14]. Notably, this time-domain approach requires a state-space model of the system. Next, a frequency domain approach is developed that only requires an FRF model.

B. Stable inversion in the frequency domain

In this section, Problem 2 is solved by using a Fourier transform approach that does not explicitly use a parametric model. The key aspect of this approach is that boundedness is guaranteed if the Fourier transforms are well defined.

Lemma 1. *Let G be a stable system satisfying* (1)*. If for a certain r, $R(\omega) = \mathcal{F}_\infty\{r(t)\}$ exists, and if $G(e^{j\omega})^{-1}R(\omega)$ is bounded $\forall \omega \in (-\pi, \pi]$, then*

$$u = \mathcal{F}_\infty^{-1}\{[G(e^{j\omega})]^{-1}\mathcal{F}_\infty\{r(t)\}\}, \tag{5}$$

is such that $u \in l_\infty$, and (1) *holds with $y(k) = r(k)$ $\forall k \in \mathbb{Z}$.*

A proof of this lemma is provided in Appendix A. This lemma shows that the DTFT-based operation (5) solves Problem 2, and only requires the FRF $G(e^{j\omega})$. Note that $G(e^{j\omega})^{-1}R(\omega)$ is bounded if $G(z)$ has no zeros on $\mathbb{C}^\circ$. This condition appears similarly in time-domain approach. Furthermore, the requirement that $\mathcal{F}_\infty\{r\}$ exists can be relaxed by adopting the notion of generalized DTFTs [14].

Remark 2. *In Lemma 1, $u(t)$ is noncausal if G is NMP. This is shown by considering $G(z)$ as the bilateral Z-transform [28, §2.13] of the impulse response of G, and $G^{-1}(z)$ as the z-component-wise inverse of $G(z)$. A bounded impulse response of $G^{-1}(z)$ is obtained by applying the inverse bilateral Z-transform over the contour $z = e^{j\omega}$, such that the region of convergence includes $\mathbb{C}^\circ$. Since $G(z)$ has no zeros on $\mathbb{C}^\circ$, this results in a bounded impulse response, which is noncausal if $G(z)$ posses zeros outside $\mathbb{C}^\circ$ [28, §2.13.2].*

In conclusion, the DTFT can be used to solve the stable inversion problem by using a continuous FRF model. Next, the DFT is considered to enable the use of a sampled FRF.

C. Periodic steady-state stable inversion

To apply the results of Lemma 1 to finite time signals, the DTFT is replaced by the DFT on a finite grid of frequencies. Truncating the infinite-time solution is exact if the involved signals are periodically repeating outside the considered time interval [28, §2.21]. Consequently, (5) can be applied by using the DFT to obtain the periodic input sequence that leads to a given desired periodic output, even if the system is NMP.

Theorem 1. *Let G be a stable system satisfying* (1) *with FRF $G(e^{j\omega_k}) = C(e^{j\omega_k}I - A)^{-1}B + D$, $\omega_k \in \Omega$,*

$$\Omega \triangleq \left\{\omega_k \in \mathbb{R} \;\middle|\; \omega_k = \tfrac{2\pi}{N}k,\ k = 0, \ldots, N-1\right\}. \tag{6}$$

If for a certain N-periodic r, $R(k) = \mathcal{F}_N\{r(t)\}$ exists, and if $G(e^{j\omega_k})^{-1}R(k)$ is bounded $\forall \omega_k \in \Omega$, then

$$u(t) = \mathcal{F}_N^{-1}\{[G(e^{j\omega_k})]^{-1}\mathcal{F}_N\{r(t)\}\},$$

is such that $u \in l_\infty$, and (1) *holds in addition to $y(k) = r(k)$ $k \in 0, \ldots, N-1$, where u and y are N-periodic.*

Proof. With the fact that $\tilde{x}(k) = \mathcal{F}_N^{-1}\{\mathcal{F}_N\{x\}\} = x(k)$ $\forall k \in \mathbb{Z}$ if x is N-periodic [28, §2.21], a proof follows identically as the proof of Lemma 1 by using $\mathcal{F}_N$ instead of $\mathcal{F}_\infty$, and by restricting u, x and y to be N-periodic signals. □

This theorem states that the bounded N-periodic input u, which results in the tracking of an N-periodic reference r, can be computed by using an FRF model of G that is defined on the DFT grid Ω (6). Note that this requires that G is in steady state, i.e., the state x is N-periodic.

In this section, the theoretical motivation for FT-IIC (3) is provided by developing a frequency domain approach to the stable inversion problem. It is shown that bounded and possibly noncausal solutions are automatically obtained by using an FRF model in combination with the DFT. Consequently, FT-IIC satisfies requirement R4. In the next section, FT-IIC is analyzed in the frequency domain.

IV. Steady-state Analysis

In this section, the convergence behavior and asymptotic properties of (3) are derived. This results in guidelines to tune $Q(k)$ and $\alpha(k)$, which constitutes contribution C2.

In the remainder of this section, it is assumed that the N-periodic steady-state output of G is measured, such that

$$Y_i(k) = G(e^{j\omega_k})U_i(k) + V(k), \tag{7}$$

where V is a bounded trial-invariant disturbance, i.e. $V_i = V$ $\forall i$. Furthermore, the dependence on k is occasionally omitted to facilitate a clear exposition.

A. Optimal FT-IIC

The FT-IIC update law, as given by (3), is shown to connect to a regularized least squares optimization problem that is commonly posed in norm-optimal ILC [2]. This reveals the particular roles of $Q(k)$ and $\alpha(k)$.

Lemma 2. *Consider the following optimization problem*

$$U_{i+1}(k) = \arg\min \mathcal{J}(k) \quad \forall k \tag{8}$$
$$\mathcal{J} = |\hat{E}_{i+1}|^2 + w_u|U_{i+1}|^2 + w_{\Delta u}|U_{i+1} - U_i|^2,$$

where $w_u(k), w_{\Delta u}(k) \geq 0$ are weights, $\hat{E}_i \triangleq R - \hat{G}U_i - V$, and $\hat{G}$ is an FRF model of G. The FT-IIC update law given by (3) *is the solution to* (8) *for*

$$Q = \frac{|\hat{G}|^2 + w_{\Delta u}}{|\hat{G}|^2 + w_{\Delta u} + w_u}, \quad \alpha = \frac{|\hat{G}|^2}{|\hat{G}|^2 + w_{\Delta u}}. \tag{9}$$

A proof of this lemma is provided in Appendix B. Considering (9) for $w_{\Delta_u}(k) = 0$ shows that $\alpha(k) = 1$ corresponds to the case where the rate of change of $U_i(k)$ is not restricted from one trial to the next. Similarly, taking $w_\Delta(k) = 0$ shows that $Q(k) = 1$ corresponds to the case where $|U_{i+1}(k)|$ is not restricted. In the next sections, additional frequency domain tuning design guidelines are derived for $Q(k)$ and $\alpha(k)$ to achieve disturbance rejection, monotonic convergence, and robustness against plant variations, respectively.

This article has been accepted for publication in a future issue of this journal, but has not been fully edited. Content may change prior to final publication. Citation information: DOI 10.1109/TMECH.2019.2931407, IEEE/ASME Transactions on Mechatronics

B. Disturbance rejection

High performance is achieved if the tracking error is sufficiently small. If the input updating (3) converges, the resulting asymptotic tracking error is as follows.

Lemma 3. *If the FT-IIC update, as given by* (3)*, converges, then the asymptotic error is given by*

$$E_\infty(k) = \frac{(1-Q(k))(R(k)-V(k))}{1-Q(k)\left(1-\alpha(k)G(e^{j\omega})\hat{G}^{-1}(k)\right)}. \tag{10}$$

A proof of this lemma is provided in Appendix C. From (10) it is clear that perfect rejection is obtained for $Q(k) = 1$. Consequently, requirement R1 is satisfied, as long as convergence is achieved with $Q(k) = 1$. Next, it is shown that this can be achieved if the FRF model is sufficiently accurate.

C. Monotonic convergence

To avoid bad learning transients [6], [33], it is key that $Q(k)$ and $\alpha(k)$ are chosen such that (3) results in monotonically converging sequences, which are defined as follows.

Definition 1. *A sequence* $\{X_i\}_{i=0}^{\infty}$*,* $X \in \mathbb{C}$*, is said to convergence monotonically in the absolute value to a fixed point* $X_\infty \in \mathbb{C}$ *if there exists a* $\kappa \in [0,1)$ *such that*

$$|X_{i+1} - X_\infty| \leq \kappa |X_i - X_\infty| \quad \forall i,$$

where κ^{-1} *is referred to as the rate of convergence.*

The following theorem provides a sufficient condition such that the FT-IIC input sequences convergence monotonically.

Lemma 4. *The sequence* $\{U_i(k)\}_{i=0}^{\infty}$*, generated by* (3)*, converges monotonically at a rate of at least* $\kappa(k) \in [0,1)$ *if*

$$|Q(k)\left(1-\alpha(k)\hat{G}^{-1}(k)G(e^{j\omega})\right)| \leq \kappa(k). \tag{11}$$

A proof to this lemma is provided in Appendix D. From (11) it is clear that both $Q(k)$ and $\alpha(k)$ can be used to achieve monotonic convergence. Note that in IIC [19], $Q(k) = 1$ such that only $\alpha(k)$ can be used to achieve convergence. In the next section, it is shown that performance can be exchanged for robustness against plant variations by taking $Q(k) \neq 1$, which is a mechanism that is lacking in pre-existing IIC approaches.

D. Robust monotonic convergence

The robust convergence requirement, R2, can be analyzed by considering the following additive uncertain model set

$$\begin{aligned} \mathcal{G}(\Delta,k) &= \hat{G}(k) + \Delta(k), \quad \Delta(k) \in \mathbf{\Delta}, \\ \mathbf{\Delta} &\triangleq \{\Delta \in \mathbb{C} \,|\, |\Delta| \leq \delta,\ \delta \in \mathbb{R}_{\geq 0}\}, \end{aligned} \tag{12}$$

where $\hat{G}$ is the nominal model and Δ is a bounded uncertainty. Such a description can be estimated by using FRF identification methods [31, §7.2.4]. By assuming that the true FRF is captured by the model set, i.e., $\exists \Delta^* \in \mathbf{\Delta}$, $G = \mathcal{G}(\Delta^*)$, robust convergence can be analyzed by substituting (12) for G in (11)

$$\begin{aligned} |Q(k)\left(1-\alpha(k)\varphi(\Delta,k)\right)| &< \kappa(k), \\ \varphi(\Delta,k) &\triangleq 1 + \hat{G}^{-1}(k)\Delta(k). \end{aligned} \tag{13}$$

More specifically, (3) is said to converge robustly with respect to (12), if (13) is satisfied $\forall \Delta \in \mathbf{\Delta}$. In case of perfect tracking, i.e., for $Q = 1$, then (13) can only be satisfied if $\varphi(\Delta) \in \mathbb{C}_{>0}$, since by definition $\alpha \geq 0$. If convergence is not achieved with respect to the true system, i.e., $\varphi(\Delta^*) \notin \mathbb{C}_{>0}$, then convergence is achieved by adjusting the phase of the nominal model by $180°$, i.e., $-\hat{G}^{-1}(k)$, since $\varphi(\Delta^*) \in \mathbb{C}_{>0}$ in this case. However, if $|\varphi(\Delta^*)| \gg 1$, (13) requires that $\alpha \ll 1$ and consequently $\kappa \approx 1$, which implies slow convergence. This is alleviated by taking $Q(k) < 1$, which increases robustness, at the cost of perfect tracking. The following lemma provides the key to achieving robust convergence by suitable design of Q and α.

Lemma 5. *If* $\exists \Delta^* \in \mathbf{\Delta}$ *such that* $G = \mathcal{G}(\Delta^*)$ *and if* $\alpha(k) \in (0,1]$*, then condition* (13) *is independent of* $\alpha(k)$*. Furthermore, if* $\alpha(k) = 1$*, then* (13) *is satisfied* $\forall \Delta \in \mathbf{\Delta}$ *if*

$$\begin{cases} Q(k) = 1 & \text{for } \tau(k) > 1 \\ Q(k) < \tau & \text{for } \tau(k) \leq 1 \end{cases}, \quad \tau(k) \triangleq \frac{|\hat{G}(k)|}{\delta(k)}. \tag{14}$$

A proof to this lemma is provided in Appendix E. In this section, it is shown that robust convergence is achieved by suitable choice of $Q(k)$ and $\alpha(k)$. Next, these results are reformulated into design guidelines.

E. Design guidelines

Based on the developed insights, design guidelines are formulated to achieve high performance and robust convergence such that requirements R1 and R2 are satisfied by FT-IIC.

The following guideline presents an approach to maximize the performance in a trial-and-error fashion when only a nominal FRF model is available.

Design Guideline 1. *Given a nominal FRF model* $\hat{G}(k)$*.*

1) *Set* $Q(k) = 1$*, and through preliminary experiments set* $\alpha(k) \in (0,1]$ $\forall k$ *as high as possible such that the input converges to a signal that is approximately identical for each trial as opposed to increasing without bounds.*
2) *If convergence is not achieved for some* k*, change the phase of* $\Delta(k)$ *by setting* $\alpha(k)\hat{G}^{-1}(k) \to -\alpha(k)\hat{G}^{-1}(k)$ *and repeat the above.*
3) *In case* $|\alpha(k)| \ll 1$ *for some* k*, set* $Q(k) < 1$ *to increase the convergence speed and robustness.*

The next guideline summarizes the approach in case robustness against plant variations is critical, or in case a trial-and-error approach is unacceptable. This requires an additive uncertain description as given by (12).

Design Guideline 2. *Given a nominal FRF model* $\hat{G}(k)$ *and additive uncertainty* $\Delta(k)$ *such that* (12) *holds. Then set* $Q(k)$ *as given by* (14) *and set* $\alpha(k) = 1$ $\forall k$*.*

In this section, the convergence behavior and asymptotic properties of (3) are derived. This results in design guidelines for $Q(k)$ and $\alpha(k)$, thereby providing an FT-IIC framework as proposed in Section II that satisfies the posed requirements.

In the next section, the effect of the transient response is analyzed in the time domain.

This article has been accepted for publication in a future issue of this journal, but has not been fully edited. Content may change prior to final publication. Citation information: DOI 10.1109/TMECH.2019.2931407, IEEE/ASME Transactions on Mechatronics

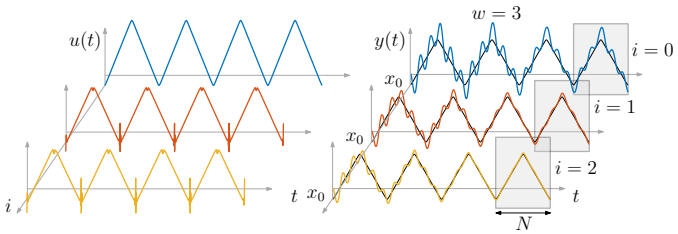

Fig. 3. In the batch-to-batch setting, each task starts from the same initial condition x_0. After w periods, a single period of N samples is measured when the system is approximately in steady state (grey intervals). The periodic input is updated based on the measured error.

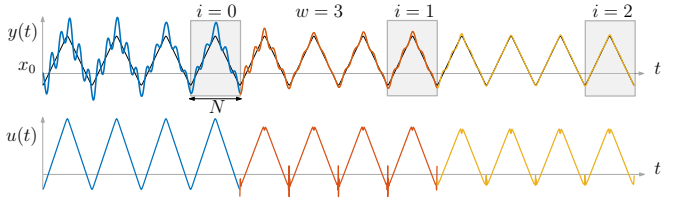

Fig. 4. In the continuous setting, the system starts from initial condition x_0, which is not reset between updates. After w periods, a single period of N samples is measured when the system is approximately in steady state (grey intervals). The periodic input is updated based on the measured error.

V. Finite-time Analysis

In the previous sections, it is assumed that the output is measured during steady state. In practice, there is a decaying contribution of the transient response that results from starting up the system, or from updating of the periodic input signal. In this section, the effects of transients are explicitly analyzed with respect to the convergence of FT-IIC. This results in conditions on the number of waiting periods w that are required to achieve convergence in the presence of transients, which constitutes contribution C3.

A. Finite time behavior

If the input to G is periodic, then the output converges to a periodic signal. Depending on the pole locations, the steady state is approximately obtained after some periods w. Hence, FT-IIC can be applied in a setting that allows for some waiting time between the input updating. In this section, two settings are considered. The first is the batch-to-batch setting, where the system resets after each update, as shown in Figure 3 for $w = 3$. The second is the continuous setting, where the system operates without resetting, as shown in Figure 4.

To analyze the transient behavior, a lifted signal description is employed that enables the consideration of an entire period at once. For a signal $s(t)$, the corresponding lifted signal $\bar{s}^{\langle n \rangle}$ is given by grouping N consecutive samples of the signal

$$\bar{s}^{\langle n \rangle} \triangleq \begin{bmatrix} s(Nn) & s(Nn+1) & \dots & s(Nn+N-1) \end{bmatrix}^\top \quad n \in \mathbb{Z}.$$

For N-periodic signals it holds that $\bar{s}^{\langle n \rangle} = \bar{s}\ \forall n$, since $s(t) = s(t+N)\ \forall t$. By lifting $u(t)$ and $y(t)$ of G as given by (1), a lifted system $G_l : \bar{u}^{\langle n \rangle} \mapsto \bar{y}^{\langle n \rangle}$ is obtained, whose realization follows by evaluating (1a), (1b) and $x(0) = x_0$ as in [34]

$$G_l : \begin{cases} x(N(n+1)) = Fx(Nn) + M\bar{u}^{\langle n \rangle}, & \text{(15a)} \\ \bar{y}^{\langle n \rangle} = Hx(Nn) + J\bar{u}^{\langle n \rangle}, & \text{(15b)} \\ x(0) = x_0, \end{cases}$$

$$\left[\begin{array}{c|c} F & M \\ \hline H & J \end{array}\right] = \left[\begin{array}{c|cccc} A^N & A^{N-1}B & \dots & AB & B \\ \hline C & h(0) & 0 & \dots & 0 \\ CA & h(1) & h(0) & & 0 \\ \vdots & \vdots & \ddots & \ddots & \vdots \\ CA^{N-1} & h(N-1) & \dots & h(1) & h(0) \end{array}\right],$$

where $h(t)$ are the Markov parameters, i.e., $h(t) = D$ for $t = 0$ and $h(t) = CA^{t-1}B$ for $t \geq 1$. This framework allows the analysis of FT-IIC in the time domain, as is treated next.

B. FT-IIC in the time domain

A number of auxiliary results are derived that enable the transient analysis of FT-IIC in the next section. First, the FT-IIC update law (3) is formulated in the lifted time domain. This requires lifting of the DFT operation, which is facilitated by the DFT-matrix $\mathcal{F} \in \mathbb{C}^{N \times N}$, i.e., $[\mathcal{F}]_{hk} = \frac{1}{\sqrt{N}}\mu^{hk}$ for $h, k = 0, \dots, N-1$, where $\mu = e^{-\frac{2\pi j}{N}}$ [35, §1.4.1]. It follows from the definition of the DFT that $\bar{S} = \mathcal{F}\bar{s}$, where $\bar{S}(k)$ results by lifting $S(k)$. Furthermore, it holds that $\bar{s} = \mathcal{F}^H\bar{S}$, since $\mathcal{F}$ is a unitary matrix [35, §4.8.1]. This formulation enables the connection of the lifted frequency domain steady-state behavior to the lifted time domain.

Lemma 6. *Given a lifted system G_l as given by* (15)*. If the state is periodic, i.e., if $x(N(n+1)) = x(Nn)$, then $\bar{y} = J_p\bar{u}$ where J_p is the periodic response matrix*

$$J_p \triangleq H(I - F)^{-1}M + J. \tag{16}$$

Furthermore, J_p is equivalent to

$$J_p = \mathcal{F}^H \mathrm{diag}\{G(e^{j\omega_k})\}\mathcal{F}, \tag{17}$$

where $\mathcal{F}$ is the DFT matrix and $G(e^{j\omega_k})$ the FRF of G.

A proof to this lemma is provided in Appendix F. This lemma enables the formulation of the FT-IIC update law (3) in the lifted time domain.

Lemma 7. *A lifted representation of* (3) *is given by*

$$\bar{u}_{i+1} = \mathcal{Q}\left(\bar{u}_i + \Lambda\hat{J}_p^{-1}\bar{e}_i\right), \tag{18}$$

$$\mathcal{Q} \triangleq \mathcal{F}^H\mathrm{diag}\{Q(k)\}\mathcal{F}, \quad \Lambda \triangleq \mathcal{F}^H\mathrm{diag}\{\alpha(k)\}\mathcal{F},$$

$k = 0, \dots, N-1$, where $\hat{J}_p$ corresponds to the FRF model $\hat{G}(k)$ and is given by Lemma 6, and $\mathcal{F}$ is the DFT matrix.

Proof of Lemma 7. Lifting (3) results in

$$\bar{U}_{i+1} = \mathrm{diag}\{Q(k)\}\left(\bar{U}_i + \mathrm{diag}\{\alpha(k)G_m^{-1}(k)\}\bar{E}_i\right).$$

Using that $\bar{S} = \mathcal{F}\bar{s}$ and $\mathcal{F}^H\bar{S} = \bar{s}$ in combination with Lemma 6 directly results in (18). □

By property of $\mathcal{F}$, the matrices $\mathcal{Q}$, Λ and J_p are circulant [35, §4.8.2], and thus correspond to time-invariant and non-causal linear mappings, as was similarly discussed in Remark 2. Furthermore, note that $\hat{J}_p$ is invertible if $\hat{G}(k) \neq 0\ \forall k$, which is in agreement with Theorem 1.

As established in Section V-A, the output used in the update can be obtained by waiting until the steady state is

This article has been accepted for publication in a future issue of this journal, but has not been fully edited. Content may change prior to final publication. Citation information: DOI 10.1109/TMECH.2019.2931407, IEEE/ASME Transactions on Mechatronics

approximately attained. To analyze the effect of remaining transients, consider the following explicit expression of the output during the w^{th} period since the input was last updated.

Lemma 8. *Given G_l as given by* (15)*. If G_l is excited by an N-periodic input $\bar{u}$, then the lifted output during the w^{th} period is given by*

$$\bar{y}^{\langle n+w\rangle} = HF^w x(Nn) + J_t \bar{u}^{\langle n\rangle}, \tag{19}$$

$$J_t \triangleq H \sum_{j=0}^{w-1} F^j M + J. \tag{20}$$

Proof. A proof follows directly by forward recursion of (15) with a periodic input $\bar{u}_i$. □

In this section, lemmas are presented that facilitate a time-domain convergence analysis of FT-IIC, as is treated next.

C. Time domain convergence analysis

Combining the auxiliary lemmas enables the main result of this section, which considers a nonconservative convergence analysis for both the batch-to-batch and continuous setting.

Theorem 2. *Let G be a stable system satisfying* (1) *and consider the tracking error given by* (2)*. If FT-IIC is used to iteratively update the input as given by* (18) *where the output is measured after waiting w periods, then the following holds.*

- ***Batch-to-batch*** *If updating is performed in a batch-to-batch fashion, as shown in Figure 3, then $\bar{u}_i$ converges if and only if $\bar{\rho}(Z) < 1$, and converges monotonically in the 2-norm if $\bar{\sigma}(Z) < 1$, with J_t given by* (20) *and*

$$Z = \mathcal{Q}(I - \Lambda \hat{J}_p^{-1} J_t). \tag{21}$$

- ***Continuous*** *If updating is performed in a continuous fashion, as shown in Figure 4, then the closed loop system is asymptotically stable if and only if $\bar{\rho}(\mathcal{A}) < 1$, with*

$$\mathcal{A} = \begin{bmatrix} F^w & \sum_{j=0}^{w-1} F^j M \\ -\mathcal{Q}\Lambda \hat{J}_p^{-1} HF^w & Z \end{bmatrix}. \tag{22}$$

Furthermore, if the model is perfect, i.e., $\hat{G}(k) = G(e^{j\omega_k})$, and if $\alpha(k) = 1\ \forall k$, then Z in (21) *and* (22) *is identical to*

$$Z_\circ = \mathcal{Q} J_p^{-1} \left(HF^w (I - F)^{-1} M \right). \tag{23}$$

A proof of this theorem is provided in Appendix G. This theorem provides conditions for the convergence of FT-IIC in the presence of transients. More specifically, in the batch-to-batch setting, stable evolution of $\bar{u}^{\langle n\rangle}$ is governed by $\bar{\rho}(Z)$. Consequently, $\bar{\rho}(Z) < 1$ provides a condition on the number of waiting periods w that are required to achieve convergence, which is typically small. To see this, consider the case where the model is perfect, i.e. Z equals $Z_\circ$, (23). Using that $\bar{\rho}(F^w) = \bar{\rho}(A)^{N \cdot w}$ where $\bar{\rho}(A) < 1$ by assumption, it follows readily that F, and therefore $Z_\circ$, converges to 0 for moderate w and N. This holds similarly for the continuous setting, in which case the matrix $\mathcal{A}$ is considered to also guarantee the stability of the state x.

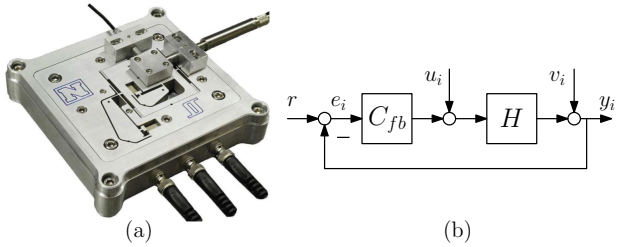

Fig. 5. (a) The three-axis nanopositioner designed by Kam K. Leang at the University of Utah. The axes contain a 12 mm long piezoelectric stack actuator of the type; Noliac NAC2003- H12, with a free displacement of 12 μm at 200 V, which is extended by mechanical amplifiers to a total range of 30 μm. Each actuator is driven by a PiezoDrive PDL200 voltage amplifier. A Microsense 6810 capacitive sensor and 6504-01 probe, with 2.5 μm/V sensitivity, is used to measure the position of the moving platform. Two SRS SIM965 analog filters serve as reconstruction- and anti-aliasing filters, respectively, by configuring these as Butterworth filters with a cut-off frequency of 3 kHz and a slope of -12 dB. (b) The closed-loop control configuration.

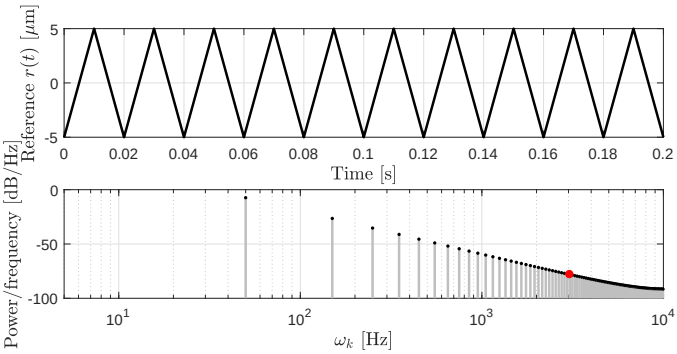

Fig. 6. Top: The reference $r(t)$ (——). Bottom: The power spectrum density of $r(t)$ (•). The point (•) indicates the contribution at ω_k^* = 3050 Hz.

Remark 3. *For $w = 0$,* (19) *satisfies $\bar{y}^{\langle n\rangle} = Hx(Nn) + J\bar{u}^{\langle n\rangle}$. Consequently, the lifted ILC problem is recovered in the batch-to-batch setting, and the lifted RC problem is recovered in the continuous setting [34]. Hence, if $w = 0$ and depending on how FT-IIC is implemented, it can be interpreted either as ILC or RC. Comparatively, FT-IIC prescribes the inverse FRF model-based learning matrix $L = \Lambda J_p^{-1}$, whereas several alternative methods exist to design this matrix for lifted ILC or RC [36]. Such methods implicitly account for the transient effects, whereas the influence of the transients is mitigated by waiting in FT-IIC, i.e., by taking $w > 0$.*

Remark 4. *In practice, a waiting time consisting of an arbitrary number of samples can be used, as long as the updated periodic input is synchronized with the original input upon application to the system. For example, by using the circular shift operation [28].*

In this section, a time-domain analysis of the developed FT-IIC is treated, which shows that convergence can be achieved in the presence of transients. In the next section, the FT-IIC approach is applied to control a nanopositioner.

VI. High Precision Periodic Nanopositioning

In this section, the potential of the FT-IIC method is demonstrated by achieving precise control of a nanopositioning stage, which constitutes contribution C4.

This article has been accepted for publication in a future issue of this journal, but has not been fully edited. Content may change prior to final publication. Citation information: DOI 10.1109/TMECH.2019.2931407, IEEE/ASME Transactions on Mechatronics

A. Control Problem

The control objective is to perform a periodic scanning motion with the x-axis of the nanopositioner shown in Figure 5(a). A single trial takes 0.2 s and consists of 10 periods of a triangle wave with an amplitude of 5 μm, shown in Figure 6. A feedback controller is used to provide a benchmark level of performance and is given by

$$C_{fb}(z) = \frac{6.1078{\cdot}10^{-6}(z{+}1)^4(z{-}0.9844)}{(z{-}0.9099)^2(z{-}0.975)(z{-}1)(z{-}0.7007)},$$

which achieves a bandwidth of 90 Hz and is operated at a sampling frequency of 20 kHz. The FT-IIC method is applied to update the feedforward signal u_i, as is shown in Figure 5(b).

B. Implementation

The FT-IIC method is implemented in a continuous setting, as presented in Section II and as shown in Figure 4. The system is first brought into continuous operation using the feedback controller. At the end of each trial a trigger indicates that data acquisition can start. In this way, sequences of exactly $N = 4000$ samples are obtained. After initialization, the input u_i is iteratively updated after three periods. The first period is used for the system to settle to steady state, i.e., $w = 1$. During the second period e_i is measured. The computation of u_{i+1} is performed during the third period by using the update law (3), wherein the DFT operation and its inverse are computed using the fast Fourier transform algorithm. Optimal time-distributed transform algorithms can facilitate computation within one sample period [37], but are beyond the scope of this exposition.

C. Application of Finite-Time IIC

In the closed-loop configuration G is the process sensitivity. The FRF estimate $\hat{G}(k) = \hat{H}(k)(1 + \hat{H}(k)C_{fb}(e^{j\omega_k}))^{-1}$ is constructed by using an estimate of the process $\hat{H}$. An H1-estimator of $H(k)$ is obtained by exciting the system with a full spectrum periodic input in open loop, and by dividing the average cross Power Spectrum Density (PSD) by the average auto PSD [31]. The resulting model $\hat{G}(k)$ and a first order approximation of its standard deviation are shown in Figure 7. This shows that for frequencies > 3 kHz, the uncertainty is relatively large. Furthermore, $\hat{G}^{-1}(k)$ is readily obtained for each k with exception of $k = 0$, since $\hat{G}(0) = 0$ due to the integrator in the feedback controller. To satisfy the condition in Theorem 1, $\hat{G}^{-1}(0)$ is set to zero.

To illustrate that high performance can be achieved with low requirements on prior modeling, Design Guideline 1 is used, since it does not require an uncertainty model. As described in step 1, $Q(k) = 1\ \forall k$, and $\alpha(k)$ is set to $\alpha_c = 0.6\ \forall k$ to allow convergence over a large frequency range. After a first exploratory experiment, it turns out that convergence is achieved up to 3700 Hz, with exception of a small set of frequencies, including $\omega_k^* = 3050$ Hz. At these non-convergent frequencies, $\alpha(k)$ is set to 0, as is shown in Figure 8. Conversely, in the lower frequency range $\alpha(k)$ can potentially be increased towards 1 at certain frequencies, which typically increases the convergence speed. This requires subsequent exploratory experiments to empirically check for convergence

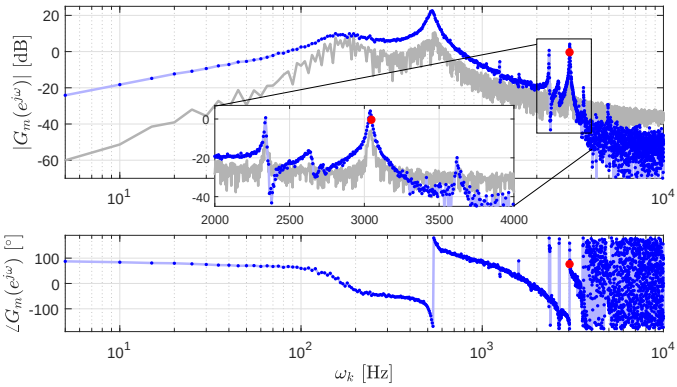

Fig. 7. Bode plot of the FRF $\hat{G}(k)$ (•), and a first order estimate of its standard deviation (——). The point (•) indicates the FRF at ω_k^* = 3050 Hz.

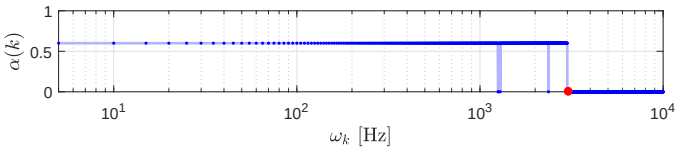

Fig. 8. The learning coefficient $\alpha(k)$ (•). The point (•) indicates the learning coefficient at ω_k^* = 3050 Hz, which is zero.

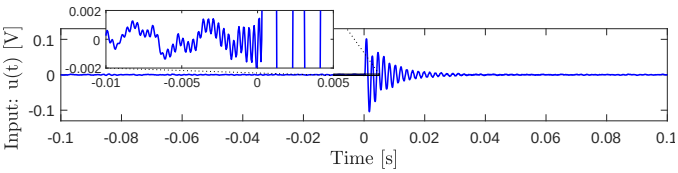

Fig. 9. The impulse response of the learning model, i.e. $\mathcal{F}_N^{-1}\{\alpha(k)\hat{G}(k)\}$ (——), shows significant noncausal behavior indicating NMP dynamics.

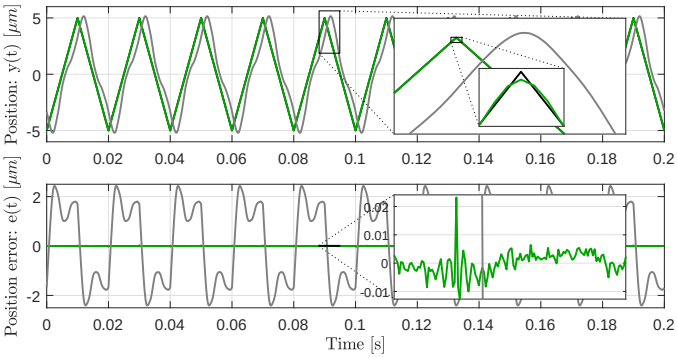

Fig. 10. Top: The reference (——), the initial output $y_0(t)$ (——), and the output after 30 FT-IIC iterations $y_{30}(t)$ (——). Bottom: Similar plot of the tracking error, which shows that converged error is about a factor 100 smaller.

and is therefore not further pursued here. To get an idea of the time domain properties of the inverse model, its periodic impulse response, $\mathcal{F}_N^{-1}\{\alpha(k)\hat{G}(k)\}$, is displayed in Figure 9. The response shows a significant noncausal contribution, which in light of Remark 2 implies that the system is NMP.

Performing the next experiment with $Q(k) = 1$ and $\alpha(k)$ as shown in Figure 8 results in a significant performance improvement, as shown in Figure 10. These plots show the output and tracking error during iteration $i = 0$ and $i = 30$. This reveals that the peak error is reduced to less than 0.5% of the reference. In Figure 11, the Root-Mean-Square (RMS) error is shown as a function of the iterations. This shows that after 7

This article has been accepted for publication in a future issue of this journal, but has not been fully edited. Content may change prior to final publication. Citation information: DOI 10.1109/TMECH.2019.2931407, IEEE/ASME Transactions on Mechatronics

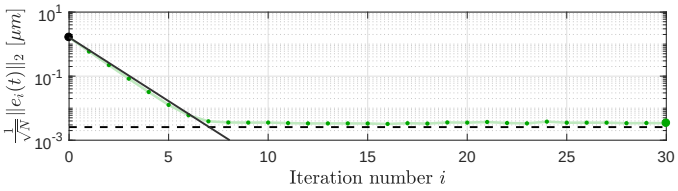

Fig. 11. The Root Mean Square (RMS) tracking error as a function of the iterations (•) shows significant performance improvement. For the first 7 iterations its behavior is proportional to the exponential 0.4^i (——), and the asymptotic value is lower bounded by the mean RMS of the non-repeating components of the error (- - -).

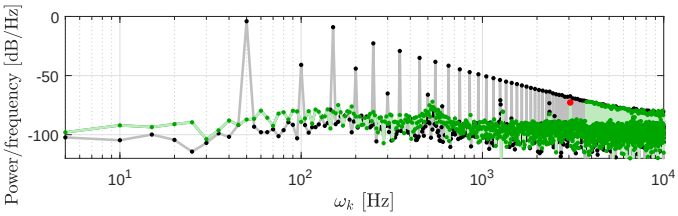

Fig. 12. The power Spectrum Density (PSD) of $e_0(t)$ (•) and $e_{30}(t)$ (•). The point (•) indicates the contribution at ω_k^* = 3050 Hz.

iterations the RMS has decreased nearly 3 orders in magnitude. During these first iterations, $\|e_i\|_2$ can be described by the exponential $0.4^i\|e_0\|_2$, which shows that the convergence rate of $\|e_i\|_2$ is approximately $\kappa^{-1} \approx 1-\alpha_c = 0.4$. Furthermore, the RMS error converges to a level that is very close to the mean RMS of the non-repeating components of the error, which is estimated by averaging 30 identical experiments. In Figure 12, the PSD of e_0 and e_{30} are shown. The PSD of $e_0(t)$ reveals contributions at $50+100\cdot n$ Hz and at $100\cdot n$ Hz, where the latter are induced by nonlinearities since these do not appear in $R(k)$. The PSD of $e_{30}(t)$ confirms that disturbance rejection is achieved for all frequencies at which $\alpha(k) \neq 0$. Notably, the largest component occurs at ω_k^* = 3050 Hz, since $\alpha(k^*) = 0$.

This frequency is specifically treated by executing steps 1 and 2 of Design Guideline 1. The result is shown in Figure 13, where each line represents the average of 40 experiments.

1) By taking $\alpha(k^*) = 0.05$ the PSD of the error diverges.
2) To achieve convergence, $\alpha(k^*)$ is reduced and the sign of $\alpha(k^*)\hat{G}(k^*)$ is changed by taking $\alpha(k^*) = -0.01$. This results in slow convergence.
3) The convergence speed in increased by increasing $\alpha(k^*)$. It turns out that $\alpha(k^*) = -0.05$ yields the best result for $Q = 1$. The convergence is relatively slow.

Since $\alpha(k^*)$ is relatively small, step 3 can be performed to increase the convergence speed by taking $Q(k^*) < 1$. Moreover, since convergence is only achievable for $-0.05 < \alpha < 0$, a large perturbation $\Delta(k^*)$ can be simulated by taking $\alpha(k^*) = -1$. By taking $Q(k^*) = 0.5$, convergence is nevertheless achieved and at a higher rate, as is clear from Figure 13. This shows that by incorporating the robustness coefficient Q, superior performance is achieved with respect to pre-existing IIC [19].

D. Comparision to data-driven learning

In this section, the FRF-based approach is compared to a data-driven approach. The latter is obtained by setting $Q(k) = 1$ and replacing $\hat{G}$ by $\hat{G}_i = (U_i(k) + C_{fb}(e^{j\omega_k}R(k)))Y_i(k)^{-1}$,

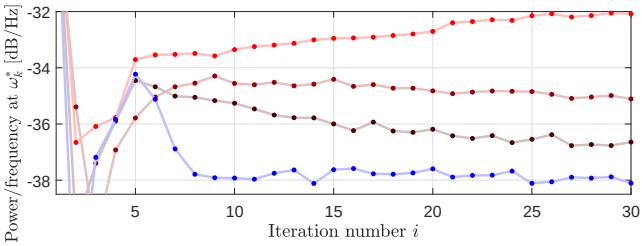

Fig. 13. The power spectrum density of the tracking error at ω_k^* = 3050 Hz during the tuning procedure, where $Q = 1$ and $\alpha = 0.05$ (•), $\alpha = -0.01$ (•), $\alpha = -0.05$ (•) and where $Q = 0.5$ and $\alpha = -1$ (•). This shows that by taking $Q(\omega_k^*) < 1$ the convergence speed can be increased, even when the model $\hat{G}$ is artificially made to be inaccurate by choosing $\alpha(\omega_k^*)$ large. Each line represents the average of 40 experiments.

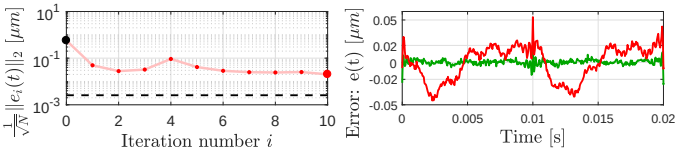

Fig. 14. Top left: The RMS error of data-driven FT-IIC (•) shows performance improvement and irregular behavior at $i = 4$ (——). Top right: the data-driven FT-IIC error is larger than the FRF-based FT-IIC error (——) at $i = 10$.

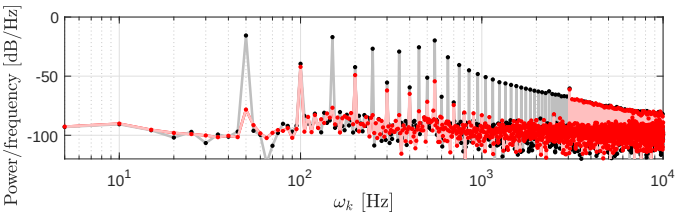

Fig. 15. PSD of $e_0(t)$ (•) and $e_{30}(t)$ (•) for MF-IIC.

where U_i and Y_i result from iteration i [22]. To avoid learning transients for small $|Y_i|$, an exponentially decreasing learning gain is used, i.e., $\alpha(k) = e^{-i/i_{\max}}\ \forall k$. The resulting performance is shown in Figure 14. Clearly, the achieved performance is inferior, which is mainly due to the fact that the data-driven approach cannot reject the nonlinear disturbances that appear at those frequencies where $R(k) = 0$, as is apparent by comparing Figure 12 and 15. Furthermore, the convergence behavior as shown in Figure 14 displays a learning transient at $i = 4$ despite the exponentially decreasing $\alpha(k)$. This indicates that more rigorous measures are required to ensure transient-free convergence, as is a subject of ongoing research [33].

In summary, the FT-IIC method is applied to a nanopositioner, which shows that broadband disturbance rejection can be achieved by using non-parametric FRF models. By following the proposed design guidelines, rapid convergence and robustness against plant uncertainties are achieved.

VII. Conclusion

In this article, the FT-IIC method is developed, which iteratively improves the tracking performance of a stable LTI process by using a nonparametric FRF estimate. It is shown that under mild conditions, FRF-based inversion results in bounded inputs, even if the system possesses right half plane zeros. In contrast to pre-existing IIC approaches, the developed approach allows for robustness against plant variations. This

is facilitated by the derivation of design guidelines based on steady-state performance and robust monotonic convergence. Furthermore, a finite-time analysis of the batch-to-batch and continuous implementations reveals that the effect of transients can readily be mitigated by waiting. The potential of the proposed approach is confirmed in experiments by application to a nanopositioner.

REFERENCES

[1] Y. Shan and K. K. Leang, "Design and control for high-speed nanopositioning: serial-kinematic nanopositioners and repetitive control for nanofabrication," *IEEE Control Syst. Mag.*, vol. 33, no. 6, pp. 86–105, 2013.

[2] J. Bolder, T. Oomen, S. Koekebakker, and M. Steinbuch, "Using iterative learning control with basis functions to compensate medium deformation in a wide-format inkjet printer," *Mechatronics*, vol. 24, pp. 944–953, 2014.

[3] D. Hoelzle, A. Alleyne, and A. W. Johnson, "Basis task approach to iterative learning control with applications to micro-robotic deposition," *IEEE Trans. Control Syst. Technol.*, vol. 19, no. 5, pp. 1138–1148, 2011.

[4] S. Hara, Y. Yamamoto, T. Omata, and M. Nakano, "Repetitive Control System: A New Type Servo System for Periodic Exogenous Signals," *IEEE Trans. Automatic Control*, vol. 33, no. 7, pp. 659–668, 1988.

[5] Y. R. Teo, A. J. Fleming, A. A. Eielsen, and J. T. Gravdahl, "A simplified method for discrete-time repetitive control using model-less finite impulse response filter inversion," *J. Dynamic Syst., Measurement, Control*, vol. 138, no. 8, 2016.

[6] D. Bristow, M. Tharayil, and A. Alleyne, "A survey of iterative learning control," *IEEE Control Syst. Mag*, vol. 26, no. 3, pp. 96–114, June 2006.

[7] S. Mishra, K. L. Barton, A. G. Alleyne, P. M. Ferreira, and J. A. Rogers, "High-speed and drop-on-demand printing with a pulsed electrohydrodynamic jet," *J. Micromechanics Microengineering*, vol. 20, no. 9, 2010.

[8] F. Boeren, A. Bareja, T. Kok, and T. Oomen, "Frequency-domain ILC approach for repeating and varying tasks: With application to semiconductor bonding equipment," *IEEE/ASME Trans. Mechatronics*, 2016.

[9] L. Blanken, F. Boeren, D. Bruijnen, and T. Oomen, "Batch-to-batch rational feedforward control: from iterative learning to identification approaches, with application to a wafer stage," *IEEE/ASME Trans. Mechatronics*, vol. 22, no. 2, pp. 826–837, 2017.

[10] K. Moore, *Iterative Learning Control for Deterministic Systems*. Springer-Verlag London, 1993.

[11] L. Blanken, T. Hazelaar, S. Koekebakker, and T. Oomen, "Multivariable repetitive control design framework applied to flatbed printing with continuous media flow," in *Conf. Decision and Control*. IEEE, 2017, pp. 4727–4732.

[12] J. van Zundert and T. Oomen, "On inversion-based approaches for feedforward and ILC," *Mechatronics*, vol. 50, pp. 282 – 291, 2018.

[13] S. Devasia, D. Chen, and B. Paden, "Nonlinear inversion-based output tracking," *IEEE Trans. Automatic Control*, vol. 41, no. 7, pp. 930–942, 1996.

[14] G. Zeng and L. Hunt, "Stable inversion for nonlinear discrete-time systems," *IEEE Trans. Automatic Control*, vol. 45, no. 6, pp. 1216–1220, 2000.

[15] M. Tomizuka *et al.*, "Zero phase error tracking algorithm for digital control." *J. Dynamics Syst. Measurement, Control*, vol. 109, no. 1, pp. 65–68, 1987.

[16] M. Tomizuka and W. Messner, "Cancellation of discrete time unstable zeros by feedforward control," *J. Dynamics Syst., Measurement, Control*, vol. 116, p. 33, 1994.

[17] Q. Zou, "Optimal preview-based stable-inversion for output tracking of nonminimum-phase linear systems," *Automatica*, vol. 45, no. 1, pp. 230–237, 2009.

[18] R. de Rozario, A. J. Fleming, and T. Oomen, "Iterative control for periodic tasks with robustness considerations, applied to a nanopositioning stage," *IFAC-PapersOnLine*, vol. 49, no. 21, pp. 623–628, 2016.

[19] S. Tien, Q. Zou, and S. Devasia, "Iterative control of dynamics-coupling-caused errors in piezoscanners during high-speed AFM operation," *IEEE Trans. Control Syst. Technol.*, vol. 13, no. 6, pp. 921–931, 2005.

[20] M. Norrlöf and S. Gunnarsson, "Time and frequency domain convergence properties in iterative learning control," *Int. J. Control*, vol. 75, no. 14, pp. 1114–1126, 2002.

[21] Y. Wu and Q. Zou, "Iterative control approach to compensate for both the hysteresis and the dynamics effects of piezo actuators," *IEEE Trans. Control Syst. Technol.*, vol. 15, no. 5, pp. 936–944, 2007.

[22] K.-S. Kim and Q. Zou, "A modeling-free inversion-based iterative feedforward control for precision output tracking of linear time-invariant systems," *IEEE/ASME Trans. Mechatronics*, vol. 18, no. 6, pp. 1767–1777, 2013.

[23] Y. Yan, H. Wang, and Q. Zou, "A decoupled inversion-based iterative control approach to multi-axis precision positioning: 3d nanopositioning example," *Automatica*, vol. 48, no. 1, pp. 167–176, 2012.

[24] Y. Wu, Q. Zou, and C. Su, "A current cycle feedback iterative learning control approach for afm imaging," *IEEE Trans. Nanotechnology*, vol. 8, no. 4, pp. 515–527, 2009.

[25] G. M. Clayton, S. Tien, K. K. Leang, Q. Zou, and S. Devasia, "A review of feedforward control approaches in nanopositioning for high-speed SPM," *J. Dynamic Syst., Measurement, Control*, vol. 131, no. 6, 2009.

[26] J. Bechhoefer, "Feedforward control of a piezoelectric flexure stage for AFM," *Proc. Amer. Control Conf.*, pp. 2703–2709, jun 2008.

[27] T. Sogo, "On the equivalence between stable inversion for nonminimum phase systems and reciprocal transfer functions defined by the two-sided laplace transform," *Automatica*, vol. 46, no. 1, pp. 122–126, 2010.

[28] L. R. Rabiner and B. Gold, *Theory and application of digital signal processing*. Englewood Cliffs, NJ, Prentice-Hall, Inc., 1975.

[29] A. Bazaei, Y. K. Yong, and S. R. Moheimani, "Combining spiral scanning and internal model control for sequential afm imaging at video rate," *IEEE/ASME Trans. Mechatronics*, vol. 22, no. 1, pp. 371–380, 2017.

[30] A. J. Fleming and K. K. Leang, "Design, Modeling and Control of Nanopositioning Systems," 2014.

[31] R. Pintelon and J. Schoukens, *System identification: a frequency domain approach*. John Wiley & Sons, 2012.

[32] R. de Rozario, T. Oomen, and M. Steinbuch, "Iterative learning control and feedforward for LPV systems: Applied to a position-dependent motion system," in *Proc. Amer. Control Conf.* IEEE, 2017.

[33] R. de Rozario and T. Oomen, "Data-driven iterative inversion-based control: Achieving robustness through nonlinear learning," *Automatica*, vol. 107, pp. 342–352, 2019.

[34] G. Pipeleers and K. L. Moore, "Unified analysis of iterative learning and repetitive controllers in trial domain," *IEEE Trans. Automatic Control*, vol. 59, no. 4, pp. 953–965, 2014.

[35] G. H. Golub and C. F. Van Loan, *Matrix computations*. JHU Press, 2013, vol. 3.

[36] D. Roover, O. H. Bosgra, and M. Steinbuch, "Internal-model-based design of repetitive and iterative learning controllers for linear multivariable systems," *Int. J. Control*, vol. 73, no. 10, pp. 914–929, 2000.

[37] J. Liu, B. Yan, and Q. Zou, "Optimal time-distributed fast fourier transform: Application to online iterative learning control—experimental high-speed nanopositioning example," *Mechatronics*, vol. 41, pp. 114–124, 2017.

Robin de Rozario received the M.Sc. degree in mechanical engineering (cum laude) from the Eindhoven University of Technology, Eindhoven, The Netherlands, in 2015. He is currently pursuing a Ph.D. degree in the Control Systems Technology group within the department of Mechanical Engineering at TU/e. His research interests include identification and learning control for high performance motion systems.

Andrew Fleming graduated from The University of Newcastle, Australia (Callaghan campus) with a Bachelor of Electrical Engineering in 2000 and Ph.D in 2004. Prof Fleming is the Director of the Priority Research Center for Complex Dynamic Systems and Control and the Precision Mechatronics Lab (www.pmtxlab.com) at The University of Newcastle, Australia. His research interests include lithography, nano-positioning, scanning probe microscopy, and biomedical devices. Prof Fleming's research awards include the IEEE MARSS Best Paper award in 2019, the ATSE Baterham Medal in 2016, the IEEE Control Systems Society Outstanding Paper Award in 2007, and The University of Newcastle Researcher of the Year Award in 2007. He is the co-author of three books and more than 200 Journal and Conference articles. Prof Fleming is the inventor of several patent applications, and in 2012 he received the Newcastle Innovation Rising Star Award for Excellence in Industrial Engagement.

This article has been accepted for publication in a future issue of this journal, but has not been fully edited. Content may change prior to final publication. Citation information: DOI 10.1109/TMECH.2019.2931407, IEEE/ASME Transactions on Mechatronics

Tom Oomen Tom Oomen received the M.Sc. degree (cum laude) and Ph.D. degree from the Eindhoven University of Technology, Eindhoven, The Netherlands. He held visiting positions at KTH, Stockholm, Sweden, and at The University of Newcastle, Australia. Presently, he is associate professor with the Department of Mechanical Engineering at the Eindhoven University of Technology. He is a recipient of the Corus Young Talent Graduation Award, the 2015 IEEE Transactions on Control Systems Technology Outstanding Paper Award, the 2017 IFAC Mechatronics Best Paper Award, and recipient of a Veni and Vidi personal grant. He is Associate Editor of the IEEE Control Systems Letters (L-CSS), IFAC Mechatronics, and IEEE Transactions on Control Systems Technology. He is a member of the Eindhoven Young Academy of Engineering. His research interests are in the field of data-driven modeling, learning, and control, with applications in precision mechatronics.

APPENDIX

A. Proof of Lemma 1

Proof. Since $R(\omega)$ exists and since $G^{-1}(e^{j\omega})R(\omega)$ is bounded on $(-\pi,\pi]$, $U(\omega) = [G(e^{j\omega})]^{-1}\mathcal{F}_\infty\{r\}$ is integrable on $(-\pi,\pi]$, and hence (5) exists, and $u \in l_\infty$. Furthermore, since $\mathcal{F}_\infty\{x(k+1)\} = e^{j\omega}\mathcal{F}_\infty\{x(k)\}$ [28, §2.2], the DTFT of (1a) equals $e^{j\omega}X(\omega) = AX(\omega)+BU(\omega)$, and since G has no poles on the unit disc, $X(\omega) = (e^{j\omega}I-A)^{-1}BU(\omega)$ is unique and bounded for any $U(\omega)$. Next consider the DTFT of (1b) $Y(\omega) = CX(\omega) + DU(\omega) = (C[e^{j\omega}I - A]^{-1}B + D)U(\omega)$, and hence $Y(\omega) = G(e^{j\omega})U(\omega) = G(e^{j\omega})[G(e^{j\omega})]^{-1}R(\omega)$, which shows that (1) holds, and $y(k) = r(k)\ \forall k \in \mathbb{Z}$. □

B. Proof of Lemma 2

Proof. Combining (7) with $E_i = R - Y_i$ and using $\hat{G}(k)$ to model $G(e^{j\omega_k})$ leads to $\hat{E}_{i+1} = \hat{E}_i - \hat{G}(U_{i+1}-U_i)$. Substituting this in the optimality condition $\frac{\partial \mathcal{J}}{\partial U_{i+1}} = 0$ results in (3) with $Q(k)$ and $\alpha(k)$ given by (9). □

C. Proof of Lemma 3

Proof. The true error is given by $E_{i+1} = \tilde{R} - GU_{i+1}$, where $\tilde{R} \triangleq R - V$. Substituting the optimal FT-IIC update law (3) in this relation gives $E_{i+1} = \tilde{R} - QG\left(U_i + \alpha\hat{G}^{-1}E_i\right) = \tilde{R} - QGU_i - Q\alpha G\hat{G}^{-1}E_i$. Rewriting E_i gives $GU_i = \tilde{R} - E_i$. Substitution of the latter in E_{i+1} leads to $E_{i+1} = (1-Q)\tilde{R} + Q\left(1 - \alpha G\hat{G}^{-1}\right)E_i$ which at the fixed point $E_{i+1} = E_i \triangleq E_\infty$ results in (10). □

D. Proof of Lemma 4

Proof. Define $\gamma \triangleq \left(1 - \alpha\hat{G}^{-1}G\right)$ and substitute (10) and E_{i+1}, as in the proof of Lemma 3, in $|E_{i+1} - E_\infty|$ to yield,

$$\begin{aligned}|E_{i+1} - E_\infty| &= \left|(1-Q)\tilde{R} + Q\gamma E_i - \tfrac{(1-Q)}{1-Q\gamma}\tilde{R}\right| \\ &= \left|Q\gamma\left(E_i - \tfrac{(1-Q)}{1-Q\gamma}\tilde{R}\right)\right| = |Q\gamma|\,|E_i - E_\infty|.\end{aligned}$$

Recalling Definition 1 completes the proof. □

E. Proof of Lemma 5

Proof. For $\tau < 1$, $\varphi \in \mathbb{C}_{>0}$ and $\Re\{\varphi\} < 2$, which implies that (13) is satisfied for all $\alpha \in (0,1]$. For $\tau \geq 1$, $\varphi \in \mathbb{C}$, i.e. the phase of φ is not restricted and consequently $\nexists\alpha$ such that (13) is satisfied. For $\alpha = 1$, (13) results in

$$|Q(k)\hat{G}^{-1}(k)\Delta(k)| \leq \left|Q(k)\frac{1}{\tau(k)}\right|$$

Hence, (13) is satisfied $\forall\Delta \in \mathbf{\Delta}$ if (14) holds. □

F. Proof of Lemma 6

Proof. Restrict the input to be periodic, i.e. $\bar{u}_i = \bar{u}$, and assume that the system is in steady state, i.e., $x(N(n+1)) = x(Nn)$. Substituting this identity in equation (15a) combined with (15b) and $x(t_0) = x_0$ yields $\bar{e}_i = \bar{r} - J_p\bar{u}_i$, where the periodic response matrix J_p is given by (17). Employing the matrix push-through identity shows that J_p is circulant. Since $\mathrm{diag}\{G\}$ is a diagonal matrix, $\mathcal{T} \triangleq \mathcal{F}^H\mathrm{diag}\{G\}\mathcal{F}$ is also a circulant matrix by property of $\mathcal{F}$ [35, §4.8.2]. Hence, it suffices to compare a single row of J_p and $\mathcal{T}$. Using $\mu^{(N-k)i} = \bar{\mu}^{ki}$ and $\frac{1}{N}\sum_{k=0}^{N-1} e^{j\omega_k h}(e^{j\omega_k} - A)^{-1} = (I - A^N)^{-1}A^{N-h-1}$, which is validated by direct computation, shows that $J_p = \mathcal{T} = \mathcal{F}^H\mathrm{diag}\{G\}\mathcal{F}$. □

G. Proof of Theorem (2)

Batch-to-batch. Consider $\bar{e}_i$ which results from the output after waiting for w periods, as is given by (19), i.e.,

$$\bar{e}_i = \bar{r} - \bar{y}_i^{\langle w\rangle} = \bar{r} - HF^w x(0) - J_t\bar{u}_i.$$

Substitution in (18) yields

$$\begin{aligned}\bar{u}_{i+1} &= \mathcal{Q}\bar{u}_i + \mathcal{Q}\Lambda\hat{J}_p^{-1}(\bar{r} - HF^w x(0) - J_t\bar{u}_i), \\ &= Z\bar{u}_i + \mathcal{Q}\Lambda\hat{J}_p^{-1}(\bar{r} - HF^w x(0)).\end{aligned} \tag{24}$$

This first order linear recursion is stable iff $\bar{\rho}(Z) < 1$. In addition, setting $\bar{u}_{i+1} = \bar{u}_i = \bar{u}_\infty$ in (24) results in the fixed point $u_\infty = (I - Z)^{-1}\Lambda\hat{J}_p^{-1}(\bar{r} - HF^w x(0))$, and it follows readily that $\|\bar{u}_{i+1} - u_\infty\|_2 = \|Z\|_2\|\bar{u}_i - u_\infty\|_2$. Recalling Definition 1, $\bar{u}_i$ converges monotonically in $\|.\|_2$ if $\|Z\|_2 = \bar{\sigma}(Z) < 1$. In case $\hat{G}(k) = G(e^{j\omega_k})$, and if $\alpha(k) = 1\ \forall k$, then it holds that $\Lambda = I$ and $\hat{J}_p = J_p$. Consequently $Z = \mathcal{Q}(I - J_p^{-1}J_t)$. Consider J_t, given by (20), $J_t = H\sum_{j=0}^{w-1}F^jM + J$, which can be written as $J_t = H\sum_{j=0}^{\infty}F^jM + J - H\sum_{j=w}^{\infty}F^jM$, which is identical to $J_t = H\sum_{j=0}^{\infty}F^jM + J - HF^w\sum_{j=0}^{\infty}F^jM$. Next, use that $\sum_{j=0}^{\infty}F^j = (I-F)^{-1}$, which holds if $\bar{\rho}(F) < 1$ [35, §11.5.6], which holds since $F = A^N$ where $\bar{\rho}(A) < 1$. Hence $J_t = J_p - HF^{-w}(I-F)^{-1}M$ where J_p is given by (16). Consequently $Z = \mathcal{Q}(I - J_p^{-1}(J_p - HF^{-w}(I-F)^{-1}M))$, which is identical to (23), thereby completing the proof. □

Continuous. Consider $\bar{e}_i$ that results after waiting for w periods since the previous input update, as is given by (19), i.e., $\bar{e}_i = \bar{r} - \bar{y}^{\langle n+w\rangle} = \bar{r} - HF^w x(Nn) - J_t\bar{u}^{\langle n\rangle}$. Next, let $\bar{u}^{\langle w+n\rangle}$ be given by $\bar{u}_{i+1}$ as given by (18), i.e.,

$$\begin{aligned}\bar{u}^{\langle w+n\rangle} &= \mathcal{Q}\bar{u}^{\langle n\rangle} + \mathcal{Q}\Lambda\hat{J}_p^{-1}(\bar{r} - HF^w x(Nn) - J_t\bar{u}^{\langle n\rangle}) \\ &= Z\bar{u}^{\langle n\rangle} + \mathcal{Q}\Lambda\hat{J}_p^{-1}(\bar{r} - HF^w x(Nn)).\end{aligned}$$

In addition, $x(N(n+w))$ follows by recursion of (15a)

$$x(N(n+w)) = F^w x(Nn) + \sum_{j=0}^{w-1}F^jM\bar{u}^{\langle n\rangle}.$$

Hence, a realization of the lifted closed loop dynamics is

$$\xi(n+w) = \mathcal{A}\xi(n) + \begin{bmatrix}0\\ \mathcal{Q}\Lambda\hat{J}_p^{-1}\end{bmatrix}\bar{r}, \quad \xi(n) = \begin{bmatrix}x(Nn)\\ \bar{u}^{\langle n\rangle}\end{bmatrix},$$

where $\mathcal{A}$ is given by (22). The closed dynamics are stable iff $\bar{\rho}(\mathcal{A}) < 1$, which concludes the proof. □